Reviews of Electromagnetics, Vol. IV, 2025
EuCAP 2025 Special Issue
DOI: 10.53792/RoE/2025/25005

Reviews of Electromagnetics
EuCAP 2025 Special Issue

Systematic methodology for cylindrical structural antenna design

Raphael Notter[1,2*], Sylvain Collardey [2], Ala Sharaiha [2], Loïc Bernard [1,2], Philippe Pouliguen [3], Paul Karmann [3]

Abstract
This paper presents a methodology for the design of cylindrical structural antennas that operate using radial modes, making them efficient radiating elements. These antennas are directly integrated into cylindrical structures making them suitable for aerospace and automotive applications. The proposed approach enables the excitation of such a structure with a low-profile source and benefits from a larger resonant surface. A major challenge of these antennas is the appearance of higher-order modes when the structure's size becomes large compared to the wavelength. However, radial modes, remain largely unaffected by the cylinder's length, making them particularly advantageous. To address this, we propose a novel method to excite radial modes on cylindrical structures with different radii and lengths. First, Characteristic Modal Analysis (CMA) is used to select the desired and undesired modes. Next, the excitation of these modes through slots is analyzed and optimized, followed by the feeding design using coaxial probes or aperture coupling feeding. Additional improvements such as parasitic slots are also explored. Different models are presented and simulations are conducted using a 3D full-wave solver. Prototypes for various sizes were fabricated. The results demonstrate that this approach enables seamless antenna integration into various cylindrical structures without compromising electromagnetic performance, even when the structure is significantly larger than the wavelength. This work highlights the potential for multifunctional systems.

Key terms
antennas; electromagnetics; platform-integrated antennas; structural antennas.

[1] *ISL: French-German Research Institute of Saint-Louis (ISL), 68300 Saint-Louis, France*
[2] *Univ Rennes, CNRS, Institut d'Electronique et des Technologies du Numérique (IETR), UMR 6164, 35042 Rennes, France*
[3] *Defense Innovation Agency (DIA), Ministry of Defense, France*
***Corresponding author**: raphael.notter@isl.eu

Received: 19/05/2025, Accepted: 23/07/2025, Published: 28/11/2025

1. Introduction

Medium-to-small flying and rolling vehicles, such as drones and ground robots, primarily rely on wireless communication. This implies the need for antenna integration on those structures, some of them being cylindrical. Antennas in these applications are required to provide reliable, high-speed data transmission and long communication ranges, while also maintaining a low profile to preserve the vehicle's aerodynamics. However, metallic platforms can interfere with antenna performance by introducing unwanted coupling. This often leads to degraded radiation characteristics. Especially when, the structure's size is comparable to or larger than the operating wavelength. This interference is mainly caused by higher-order modes that are excited on the platform surface [1]. A solution is the use of structural antennas or platform-integrated antennas, which generate the desired radiation pattern by directly exciting its platform [2]. In this case the carrier effects are already taken into account and, even better, it is possible to take advantage of the larger radiating surface and the multiple modes present to increase the antenna's communication performance. In the case of cylindrical structures, several techniques have been proposed in the literature, such as exciting the cylinder like a dipole [3]. This works efficiently when the length of the cylinder is comparable to the wavelength. However, this becomes ineffective when the cylinder is significantly longer. Alternative methods such as using loaded wire radiators [4] or external half loops [5], have also been proposed, but these are not compatible with the low-profile requirements emphasized in this work. It could be

Number	Radius (R)	Length (L)	frequency (f_c)
Design #1	$0.24\lambda_c$	$1.2\lambda_c$	3.6 GHz
Design #2	$0.57\lambda_c$	$6.5\lambda_c$	4.3 GHz
Design #3	$0.62\lambda_c$	$3.8\lambda_c$	2.3 GHz

Thickness (T)	Desired Mode
2 mm	Radial J_1
2.5 mm	Radial J_1
3 mm	Radial J_0

Table 1: Design dimensions

possible to combine several modes to obtain the desired radiation pattern [6, 7]. It is also possible to excite the radial modes that are not perturbed by the length dimension [8]. Until now the authors have studied this approach using different modes, excitation techniques and cylinder dimensions [9, 8]. But no systematic method exists to excite these kinds of modes with the advantages and disadvantages which result from it. Hence, this paper addresses this gap by presenting a structured approach to implementing cylindrical structural antennas based on radial modes. Three hollow cylinders of arbitrary chosen radii (R), central frequencies (f_c), length sizes (L) and thicknesses (T) are investigated for our designs. Design #1 works at 3.6 GHz and has a length of 100 mm ($1.2\lambda_0$), a radius of 20 mm ($0.24\lambda_0$) and a thickness of 2 mm. Design #2 works at 4.3 GHz, has a radius of 40 mm ($0.57\lambda_0$), a length of 450 mm ($6.5\lambda_0$) and a thickness of 2.5 mm. Design #3 works at 2.3 GHz, has a radius of 80 mm ($0.62\lambda_0$), a length of 500 mm ($3.8\lambda_0$) and a thickness of 3 mm. Designs #1 and #2 were simulated and prototyped whereas design #3 was only simulated. All the design characteristics are summarized in Table. 1, the parameters and hollow cylinder model are shown in Fig. 1. Section 2 details the methodology, including mode selection, slot optimization, and structure design. Section 3 presents the simulation results, fabrication details, and prototype measurements. Before concluding, a summary of the study and a discussion of the results obtained are presented in section 4.

2. Design Methodology: Modal Analysis Based Approach

All Characteristic mode analysis (CMA) and Full wave simulations were carried out using the CST Studio suite 2024 and more specifically the integral and frequency domain solver respectively [10].

2.1. Modal analysis

The theory of characteristic modes has its origins in the initial work of Garbacz [11] and was later refined by Harrington and Mautz [12]. According to the method, the complex matrix Z from the method of moments, expressed as R + jX can be decomposed into a set of characteristic currents J_n and corresponding λ_n eigenvalues by solving the following equation:

$$XJ_n = \lambda_n RJ_n \tag{1}$$

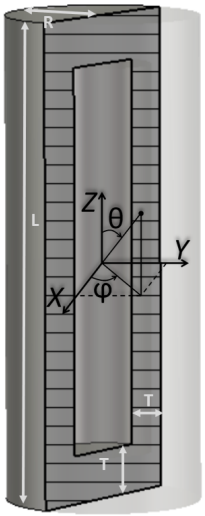

Figure 1: Parameters and view of considered cylinders

The following parameters can be used in order to select a specific mode :

- **Characteristic currents** (J_n):

  These are the electromagnetic currents which circulate on the surface of the structure in response to electromagnetic excitation. The characteristic currents depend only on the geometry of the structure and the operating frequency.

- **Eigenvalues** (λ_n):

  Eigenvalues are scalar numbers that represent the natural resonance properties of a characteristic mode. When its value reaches 0, the mode is resonant at the associated frequency. To avoid confusion with the wavelength, it will be denoted as λ_c, while eigenvalues will be represented as λ_n.

After applying CMA to the designs, the observed modal behavior is difficult to analyze, multiple modes are resonant. In fact, because of the large dimensions of the antenna compared to λ_c (see Table. 1), all the antennas have multiple resonating modes (eigenvalues close to zero) and more than 50 modes in the worst case of design #2 (Fig. 2b). In the case of design #1 (Fig. 2a), fewer resonant modes are observed; however, the eigenvalue of the desired mode (Mode 19) is closer to -3 rather than zero. This means that, in addition to the prominent presence of higher-order modes, the desired mode will be more difficult to excite effectively at the operating frequency.

2.2. Proposed mode classification

Rather than analyzing each mode individually, the adopted approach focuses on identifying the key characteristics of the modes, classifying them into mode types to simplify the analysis, and selecting only those most relevant to the application. As a result of this, three proposed types of modes were identified:

- **Dipolar modes** modes of the dipole antenna where current are focalized along the length of the cylinder. It is possible to visualize the dipolar modes by considering the

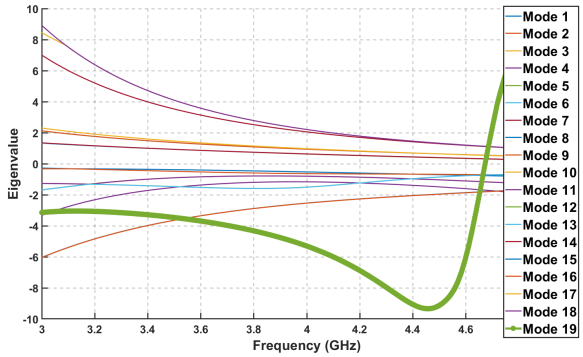

(a) Eigenvalues of design #1

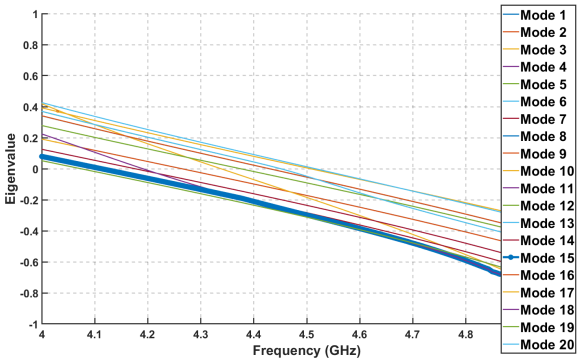

(b) Eigenvalues of design #2

Figure 2: Eigenvalues of design #1 and #2

cylinder as a thick dipole. Both the $\lambda/2$ and λ harmonics have been used for a structural antenna application as shown in [3]. The λ harmonic current and far field are represented in Fig. 3.

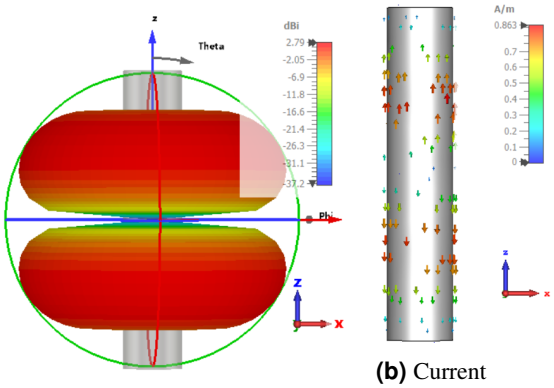

(a) Radiation pattern of dipolar λ mode

(b) Current distribution of dipolar λ mode

Figure 3: Far field and current distribution of dipolar λ mode

- **Radial modes** modes of the loop antenna or magnetic dipole [13], where currents are concentrated in the radial direction of the cylinder. It is possible to visualize the radial modes by considering the cylinder radius as a thick loop or an assembly of loop resonators. These kind of modes were used by the authors previously [8, 9]. The J_0 harmonic current and far field are represented in Fig. 4 and the J_1 harmonic is represented in Fig. 5.

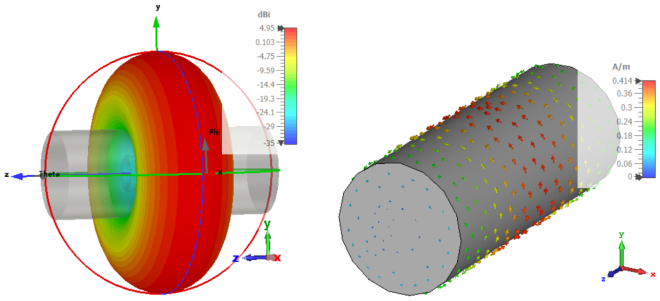

(a) Radiation pattern of Radial J_0 loop mode

(b) Current distribution of Radial J_0 loop mode

Figure 4: Far field and current distribution of radial J_0 loop mode

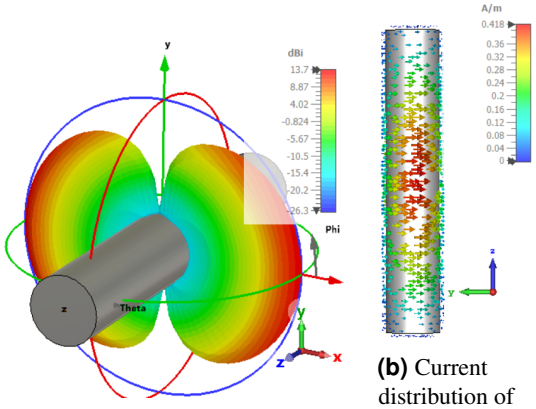

(a) Radiation pattern of Radial J_1 loop mode

(b) Current distribution of Radial J_1 loop mode

Figure 5: Far field and current distribution of radial J_1 loop mode

- **Longitudinal modes** where the current flows from one end cover of the cylinder to the other and returns along the cylinder's length. These modes can be visualized by considering the perimeter of the cylinder along its axial direction as forming a continuous loop. However, longitudinal modes, due to the influence of the end covers, differ from conventional loop modes. Due to their more complex behavior, such modes have, to the authors' knowledge, not yet been utilized in structural antenna applications. The J_0 harmonic current and far field are represented in Fig. 6.

The list presented above is not exhaustive; in fact, certain modes were found to exhibit characteristics belonging to multiple categories simultaneously (Fig. 7). These modes are referred to as hybrid modes, as they can be interpreted as a combination of the three previously identified mode types. Such hybrid modes typically appear at higher orders.

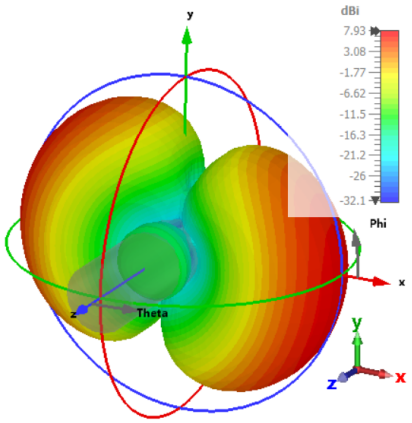

(a) Radiation pattern of longitudinal J_0 mode

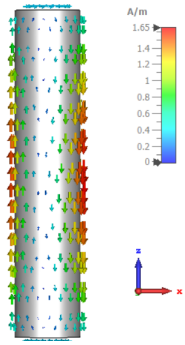

(b) Current distribution of longitudinal J_0 mode

Figure 6: Far field and current distribution of longitudinal J_0 mode

2.3. Proposed Methodology

For the first step of the modal analysis, a parametric study using CMA is conducted. To ensure generality and independence from the operating frequency, all quantities are now expressed as fractions of the wavelength. The corresponding dimensions normalized to the wavelength are shown in Table. 1. The analysis proceeds by examining each of the four designs individually, varying their radii, and applying CMA at each radius. This process yields the modal distribution for every radius of each design. The modes are sorted based on the corresponding design's operating frequency, f_c.

The objective is to study how the modal distribution evolves with radius and to identify potential patterns in the emergence of specific mode types. For each radius, the first ten modes are extracted and classified into the three previously defined categories: dipolar, radial, or longitudinal. This classification is based on the eigenvalues at the sorting frequency. In this context, "Mode 1" refers to the mode whose eigenvalue is closest to zero, indicating that it is the most resonant. Results are partially shown in Fig. 8. Firstly, there are three subgraphs, each corresponding to one of the designs. Secondly, for each subgraph, the mode appearance order is plotted on the y-axis as a function of the cylinder radius. However, only three points are shown per radius value. This is because only the appearance order of the first mode of each type (dipolar, radial, and longitudinal) is represented. In other words, only the appearance order of the first dipolar mode (the dipolar mode with the eigenvalue closest to zero) is computed. The same is done for the first radial and first longitudinal modes. For example, the length of design #3 is equal to 3.8 wavelengths, corresponding to Fig. 8b. For a radius equals to λ_c, the first dipolar mode to appear on Design #3 is at position 1, the first longitudinal mode at position 2, and radial mode at position 4. Position 3 also corresponds to a longitudinal mode (a degenerate of mode 2), but since a longitudinal mode has already been identified, all subsequent harmonics of this type are skipped until the first radial mode is found, which occurs at position 4 in this case. This choice was made to clearly identify the onset of each mode type, regardless of their harmonics. It allows evaluating whether a particular mode type appears among the first ten modes for a given radius in each design.

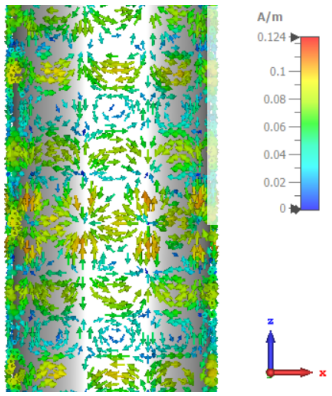

Figure 7: Example hybrid mode current distribution

Each designs listed in Table. 1 corresponds to a specific radius in the corresponding figure and is marked with a circle. To determine whether certain mode types are more resonant at specific dimension ranges, the analysis focuses on which mode type appears earlier than the others across a sufficiently broad radius interval. If a given mode type consistently emerges first, it is considered predominant within that region of the graph. For example, in the case of design #1 (Fig.8a), which corresponds to a cylinder length of $1.2\lambda_c$, and a radius of $0.24\lambda_c$, the design lies within a region where dipolar modes are predominant. Design #2 (Fig.8c) falls within a radial predominance region. Design #3 (Fig.8b) is located in a longitudinal predominance zone. These examples demonstrate that the designs are distributed across three different modal predominance regions. The goal is to demonstrate that designs can be implemented within any of these modal regions, and that the proposed method remains systematic and applicable regardless of the modal context.

Thanks to the graphs, three observations can be made:

1. For all cylinder lengths, the dipolar mode type dominates when the radius is small compared to the wavelength.
2. Radial and longitudinal mode predominance does not occur for all lengths.
3. For each length, there are regions where no single mode type is predominant.

Radial modes, due to their highly localized current distribution, exhibit minimal sensitivity to changes in the cylinder length. [8]. This implies that radial modes can still be effectively excited, even in the presence of other highly resonant and more predominant mode types, if the focus remains solely on the radial dimension. In the mode study, except for hybrid modes that are predominant only in very higher order mode cases (at more than $1.15\lambda_c$ of radius in the $6.5\lambda_c$ of length case), radial modes are the ones with current directed primarily along this dimension. Therefore, by focusing on them, longitudinal and dipolar modes are filtered out of the CMA analysis.

The second step of the modal analysis involves the selection of suitable radial mode harmonics. For a structural antenna

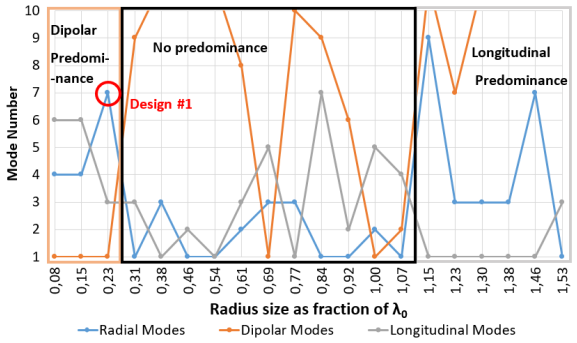

(a) Mode type predominance @$1.2\lambda_c$ of length

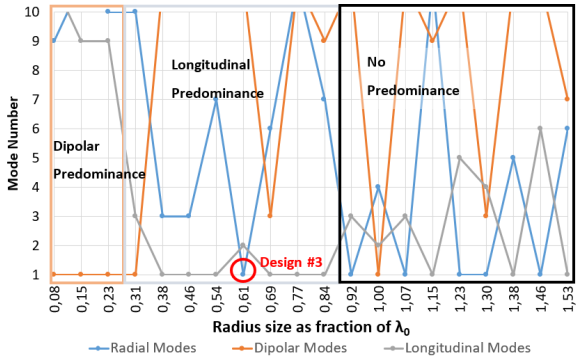

(b) Mode type predominance @$3.8\lambda_c$ of length

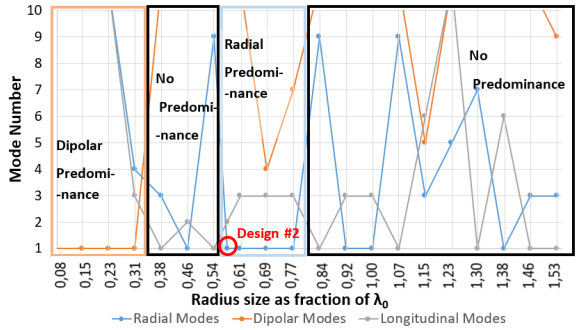

(c) Mode type predominance @$6.5\lambda_c$ of length

Figure 8: Mode type predominance for the three designs length

design to be practical, the corresponding current distribution must remain relatively simple, with a limited number of current maxima and well defined flow directions.

Based on these criteria, two radial modes harmonics were selected :

- **Radial omnidirectional mode** (J_0 loop mode [13]) : In this mode, surface currents circulate uniformly around the cylinder's circumference maintaining the same amplitude and phase. This results in a magnetic dipole-like current distribution that produces an omnidirectional radiation pattern (Fig. 5). This mode was selected for design #3 to achieve an omnidirectional pattern on a large radius design.
- **Radial J_1 loop mode** : Similar to a J_1 loop mode [14], currents flows from one side of the cylinder to the other (Fig. 5b) exhibiting two current maxima on each side. The associated radiation patterns consist of two wide lobes in the plane perpendicular to the cylinder axis, with negligible side lobes, similarly to [8]. This mode was chosen for designs #1 and #2.

2.4. Mode excitation

The second step of the proposed systematic methodology is excitation of the selected radial mode (J_0 and J_1). In the literature, three main feeding techniques are commonly employed: inductive coupling elements (ICE) [15], capacitive coupling elements (CCE) [16] and direct coupling [17]. According to [17], direct coupling is achieved by making narrow slots positioned at locations where the characteristic mode current reach its maximum amplitude with the slot orientation orthogonal to the local current direction. This method effectively imprints the desired current distribution onto the structure's surface, enabling targeted mode excitation. For designs #1 and #2, which utilize the J_1 radial loop mode, the presence of two maxima necessitates the use of at least two slots to excite the mode. In contrast, only one slot is needed for the J_0 radial mode (design #4) due to the current homogeneous amplitude and phase. However, in practice it is often not sufficient, the circumference size being approximately $1.4\lambda_c$ for design #1, $3.6\lambda_c$ for design #2 and 3.9 λ_c for design #3 (radius of respectively approximately $0.24\lambda_c$, $0.57\lambda_c$ and $0.62\lambda_c$), the desired mode is sharing the excitation with other radial higher order modes (the J_1 radial is even considered a higher order when compared to the J_0 radial desired mode for the large design), a way to suppress those has to be found. In theory there are two different solutions to do it [2] :

- Suppress higher-order modes through structural modification, thereby breaking their continuity.
- Reinforce the desired mode by using multiple excitation points to increase its dominance.

Both approaches are explored and demonstrated in the next sections.

2.4.1. Excitation of design #1

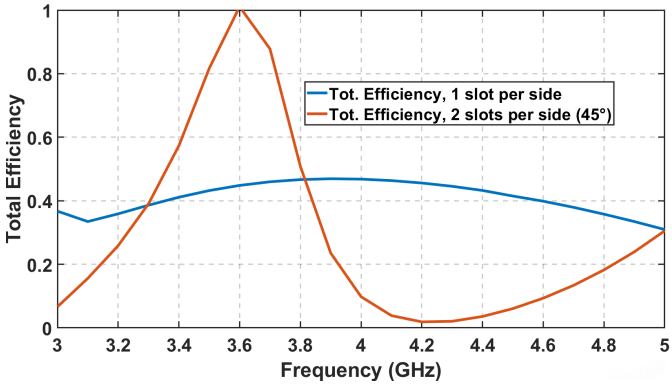

Figure 9: 1 slot vs 2 slots per side total efficiency

For design #1 (20 mm radius corresponding to $0.24\lambda_c$), using only one slot per cylinder side (two slots in total) to excite the J_1 radial mode results in a total efficiency that does not exceed 80% as shown in Fig. 9. The limited performance

Mode Number	Mode λ_n	Mode type	Harmonic
1	-0.4	Dipolar	λ
2	-0.5	Dipolar	$\lambda/2$
3	-0.83	Longitudinal	J_2
4	-0.84	Longitudinal	J_2
5	0.86	Radial	J_0
6	0.86	Longitudinal	J_0
7	0.86	Longitudinal	J_0
8	1.26	Longitudinal	J_1
9	1.26	Longitudinal	J_1
10	1.34	Radial	$2*J_0$
11	-1.37	Dipolar	1.5λ
12	-1.52	Radial	$2*J_1$
13	-1.52	Radial	$2*J_1$
14	3.13	Radial	$3*J_0$
15	-3.34	Radial	J_2
16	-3.35	Radial	J_2
17	3.57	Longitudinal	J_4
18	3.57	Longitudinal	J_4
19	-3.69	Radial	J_1

Table 2: Modes mores resonant than J_1 @3.6 GHz for design #1

indicates that the imprinted current is insufficient to generate the desired mode. Two main factors contribute to this limitation :

1. As shown in Fig. (Fig. 2a), the eigenvalue of the J_1 radial mode at 3.6 GHz is -3.69, which is significantly distant from zero. This indicates that the mode is not strongly resonant at the operating frequency

2. As reported in Table. 2, 18 modes exist at the desired frequency including seven modes of the same type. This means that the desired J_1 radial mode is in competition with multiple other modes for excitation, further reducing its dominance.

To overcome these drawbacks, a more selective excitation approach is required. As detailed in part 3.2, additional feeding slots can be strategically placed in locations that are incompatible with the current distributions of the undesired modes but compatible with the J_1 radial mode. This technique enhances coupling with the J_1 radial mode while suppressing interference from the others. Consequently, a minimum of two slots per side (4 in total) is necessary to achieve efficient excitation of the J_1 radial mode (Fig. 10).

The slots are located at 45 degrees from the center (angle A_s). Each slot measures 50 mm in length (0.6 λ_c) and 5 mm in width (0.06 λ_c). The excitation is implemented using aperture coupling feeding via microstrip lines placed on the inner wall of the cylinder (Fig. 11). A serial configuration is used for the feeding network. The two slots located in the $x > 0$ region are fed in phase by a single port, while the slots on the opposite side ($x < 0$) are fed with opposite phase by the second port. The coupling is produced by a microstrip line located in front of the slots on the inner walls of the cylinder. The coupling feeding mechanism will be detailed in part 2.3.2. To justify the choice of dimensions, a parametric study of the 3 parameters has been conducted and summarized below.

Table 3: Parametric study of L_s

L_s (mm)	20	30	40	50	60	70
f_c (GHz)	4.9	3.15	4.2	3.61	3.5	3.39
BW (MHz)	63	71	150	143	132	159
S_{21} (dB)	-7	-5	-22	-20	-14	-9
Correct mode ?	No	No	Yes	Yes	Yes	Yes

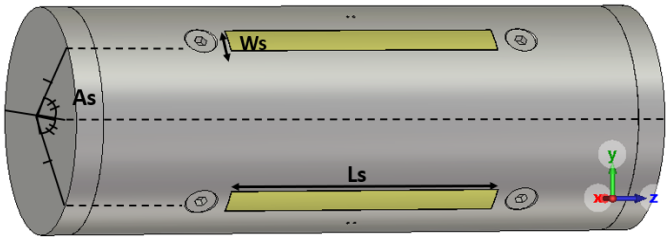

Figure 10: Slot geometry of design #1

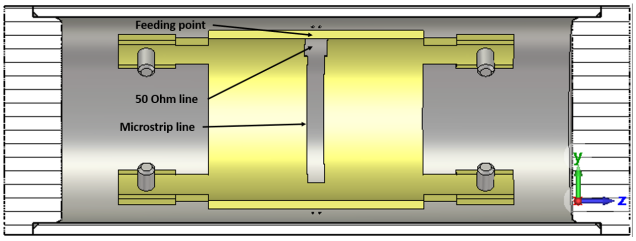

Figure 11: Dimensions of the serial microstrip feeding

- **Slot length (L_s):**

The slot width was fixed to 5 mm and its angular position relative to the center to 45 degrees (Fig.10). The results are given in Table. 3. The center frequency f_c was tracked as well as the bandwidth (BW), the coupling between ports (S_{21}) and if the correct mode is obtained or not.

Table. 3 indicates that the coupling is less than -20 dB for 40 and 50 mm. This is a satisfactory improvement compared to [8]. It can also be observed that the frequency decreases inversely with the length of the slots when the desired mode is formed. Therefore, a slot length of 50 mm is chosen to achieve the correct center frequency.

- **Slot Width (W_s):**

The slot length was fixed to 50 mm and its angle to 45 degrees (Fig.10). After rematching, the results are in Table. 4. The center frequency *fc* was tracked as well as the bandwidth (BW) and the coupling between ports (S_{21}) and whetever the correct mode was obtained or not.

It can be observed in Table. 4 that the coupling is effective for widths of 4 and 5 mm, but deteriorates once the width

Table 4: Parametric study of W_s

W_s (mm)	1	2	3	4	5	6
f_c (GHz)	2.98	3.24	3.15	3.5	3.61	4.17
BW (MHz)	17	70	85	109	143	149
S_{21} (dB)	-1	-2	-5	-27	-20	-10

Table 5: Parametric study of A_s

A_s (mm)	0	15	20	30	40	45
f_c (GHz)	0	3.611	3.622	3.6	3.61	3.61
BW (MHz)	0	277	282	249	186	149
S_{21} (dB)	-2	-26	-25	-21	-27	-20

exceeds 6 mm. Furthermore, the frequency increases with width, but not as much as with L_s. A good bandwidth, coupling and center frequency are obtained for the 5 mm value.

- **Angle of slot (A_s):**

The slot length was fixed to 50 mm and its width to 5 mm (Fig. 10). After rematching, the results are presented in Table. 5. The center frequency f_c was tracked as well as the bandwidth (BW) and the coupling between ports (S_{21}).

In Table. 5 it can be observed that the coupling is good for all angles except 0 degrees (1 slot per side). It shows again that 2 slots per side is the minimum needed to imprint the currents and excite resonance in the structure. The frequency does not change much, serving more as an matching parameter. The coupling also always stay under -20 dB except for 0 degrees. Please note that for 15, 20 and 30 degrees, a microstrip width (W_s) of 1 mm is needed. This would be harder to manufacture with the available resources, hence it was decided to push them aside for the prototype. Finally, the choice to use the 45 degrees configuration was made, even if it is the worst one, for future reconfigurability tests. It can also be seen on Fig. 9 that total efficiency exceeds 95 % for this angle.

2.4.2. Excitation of design #2

For design #2, the circumference is more than 3.6 bigger than λ_c, higher-order modes are certain to appear. The objective is to suppress them. The desired mode can be excited by placing a slot at the radial current maxima of the J_1 radial mode (Fig. 5b) and directing it towards the circumference. In addition, the characteristic currents are symmetrically identical with a maximum on each side. In this case, the mode must be excited using two minimum in-phase direct feeders that are oriented in the same direction similar to design #1. In order to increase coupling between the slots and the J_1 radial mode, H-shaped slots were used. Dimensions of the slot W_s and L_s as seen in Fig. 12 were determined by a parametric study (Table. 6) :

- W_s plays an impedance role. The bandwidth increases when W_s diminishes. However, a trade-off between feasibility and bandwidth has to be found, a slot too thin is not practically realizable.

L_s (mm)	34	36	38	40
f_c (GHz)	4.5	4.37	4.26	4.18
(W_s = 1.6 mm)				
W_s (mm)	1.2	1.4	1.6	1.8
BW (MHz)	185	237	254	251
(L_s = 38 mm)				

Table 6: Parametric study of L_s and W_s and their influence on center frequency and bandwidth

- L_s allows us to tune the resonant frequency. It decreases when L_s increases.

The final dimensions selected for the slot are W_s = 1.6 mm (0.02 λ_c) and L_s = 38 mm (0.55λ_c) .

The optimized dimensions chosen for the H shapes are 2 mm in width (W_h) and 3 mm in length (L_h). The H shapes enhance compactness, improve impedance matching, and better concentrate current in a specific direction, as observed in [3].

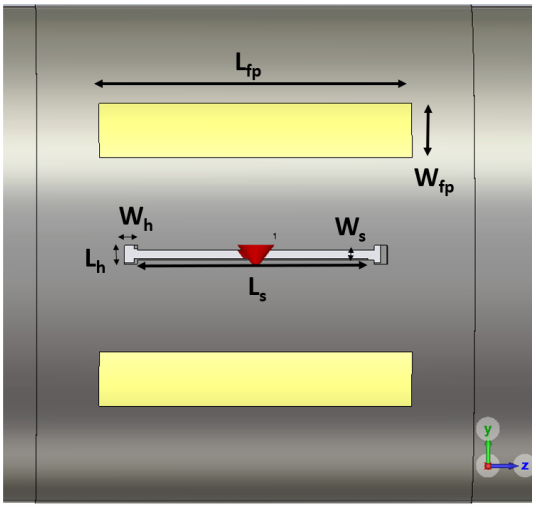

Figure 12: Design #2 parameters

- **Adding parasitic slots**

However, when implementing this solution, undesired lobes are obtained (Fig. 13) which are due to a higher radial mode fed on the circumference. Contrary to the previous design (#1), the size of the circumference being $3.6\lambda_c >> \lambda_c$, the appearance of a higher-order mode is more than probable.

As seen before in part 2.2, the two solutions to reduce the effects of this additional mode is to add feeders, or modify the structure (for example by adding parasitic slots). The second solution was chosen using 4 polyethylene ($\varepsilon_r = 2.26$) filled parasitic slots of dimensions 50 × 10 × 2.5 mm (in yellow on Fig. 10 and 12). In order to get the best results possible, it is required to place them at the maxima of the undesired mode. The optimal position was determined through a parametric study (Fig. 14) by rotating each slot by an angle A_{fp}=30° around the cylinder from the $\phi = 0$ reference position. The current maxima are subsequently suppressed, as shown in Fig.15.

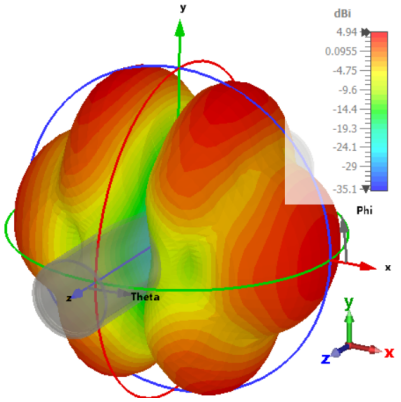

Figure 13: Design #2 3D radiation pattern disturbed by higher-order mode at 4.3 GHz

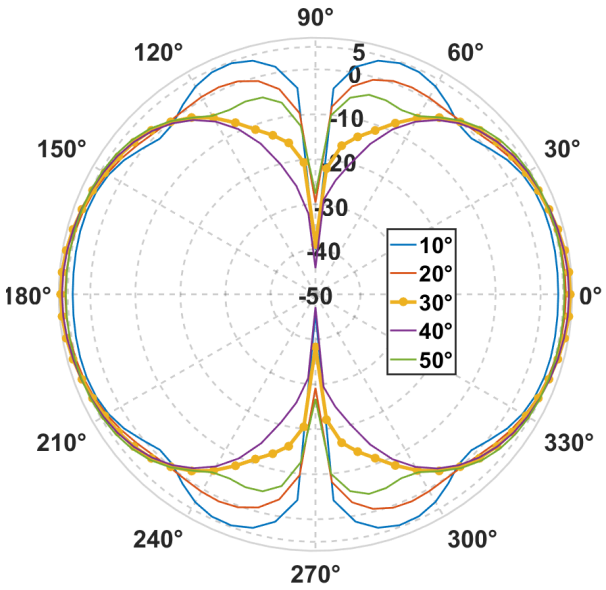

Figure 14: Parametric study of A_{fp}

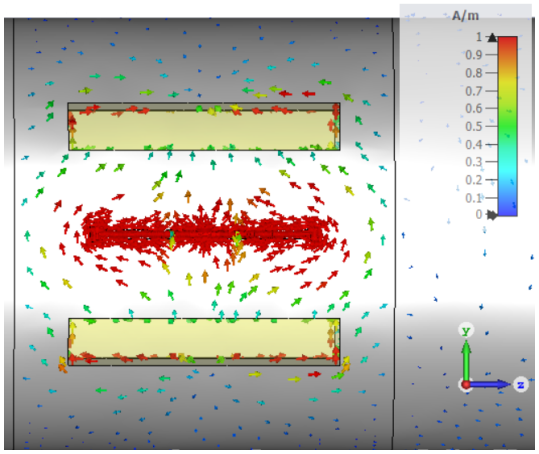

Figure 15: Current distribution of Design #2 with parasitic slots

2.4.3. Excitation of design #3

For Design #3, since the radius is approximately $0.62\lambda_c$ (corresponding to a circumference of $3.9\lambda_c$), resonant higher-order modes are expected to be present, similar to Design #2. Moreover, in design #3 case, the desired mode is the J_0 omnidirectional radial mode which is the fundamental radial loop mode. A parametric study is now conducted in order to identify how many slots are needed to enforce the desired mode. Due to the homogeneous current distribution in both phase and amplitude of the mode, it is possible to sequentially etch slots around the cylinder's circumference until the J_0 mode is identified in the simulation. Only the radiation pattern will be studied in this step. The slots have a length of 65 mm ($\lambda_0/2$) and a width of 5 mm. The slots are placed equidistantly from each other along the radial dimension. This ensures a homogeneous current distribution and maintains the symmetry of the mode.

Number of slots	Mode type	Max directivity
1	Half hemisphere	5.6
2	Higher order	5.4
3	6 Radial Lobes	5.6
4	4 Radial Lobes	7.4
5	6 Radial Lobes	5.5
6	10 Radial Lobes	4.5
7	J_0 Radial Omnidirectional	2
8	J_0 Radial Omnidirectional	2.4

Table 7: Slot number parametric study

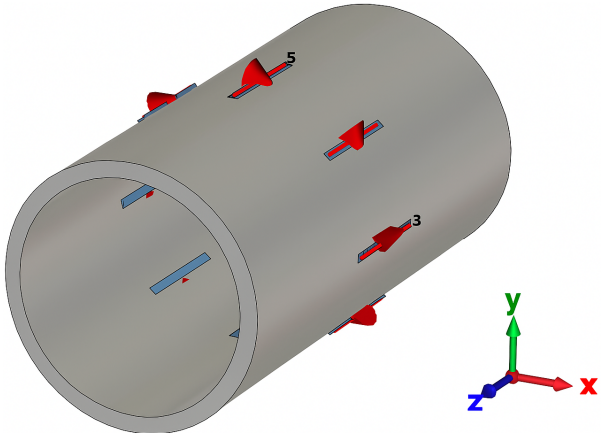

Figure 16: Placing slots on design #3

It is possible to quickly estimate the number of slots by looking at the circumference/wavelength ratio. For $3.9\lambda_c$, so approximately $4\lambda_c$, the highest order mode that can appear will have 8 extrema. Then, 8 slots would be needed in order to remove these extrema and force a homogeneous current distribution.

Table. 7 shows the slot number parametric study. A number of 7 slots minimum are needed for the correct mode generation. However, due to fabrication constraints, the configuration with 8 slots is selected.

2.5. Slot feeding design

For the last design step, slots need to be fed in order to excite the desired mode: this is possible using several techniques. In

this article, direct coaxial feeding and aperture coupled feeding (with serial and shunt feeding) will be explored in sections 2.5.1 and 2.5.2 respectively.

2.5.1. Direct coaxial feeding

The design #2 was fed by applying discrete ports to the slot. This approach induces a potential difference on each side and represents the center feeding method typically used for conventional slot antennas [18]. In practice, this is equivalent to soldering a coaxial cable onto the slot, with the center conductor connected to one side of the slot and the ground to the other side. The slot was matched only by modifying the slot dimensions and the H-branches dimensions. It is also possible to move the feed point along the slot for this. In order to feed all the slots in phase, both cables are connected to a Wilkinson splitter. No additional matching circuit are necessary. The advantage of this technique is its simplicity of realization, soldering the cables is sufficient. However, as it will be seen in section 3, this technique is pretty unstable and even more in a higher-order mode environment. In fact, if the soldering is not perfectly symmetrical, there is a possibility of exciting dipolar or longitudinal modes, that impacts the S-parameter and/or radiation pattern. Moving the cables also strongly impacts these parameters, which reduces reproducibility.

2.5.2. Aperture coupled feeding

To excite multiple slots simultaneously, rather than having multiple coaxial solderings, it is possible to feed the slots using aperture-coupled feeding. There is two main way to do it, serial (for the design #1, with small radius) or shunt (for the #3, with large radius) feeding.

2.5.2.1. Design 1 (serial feeding)

For design #1, it is necessary to feed 4 slots, with both side of the cylinder being opposed in phase, 2 microstrip lines are needed, with 2 slots fed in serial per microstrip line. It is also possible to feed both at the same time by controlling the phase shift on the line but this is not done here. The objectives would be to keep 2 ports for future reconfigurability purposes. The serial feeding design is composed of 4 components:

- a microstrip line placed on a substrate. The line is 33 mm long and 3 mm wide. This line width is corresponding to a characteristic impedance of 68 Ohms and was chosen via parametric sweeps for the matching. The substrate is polyethylene ($\varepsilon_r = 2.26$), with dimensions of 38 mm × 38 mm and a thickness of 1.6 mm. The line will pass orthogonaly below the slot to feed them via coupling. It will also have a small extension after the last slot for matching purposes. This element is 3D printed.
- A slotted ground plane. Here the ground plane is the cylinder inside wall.
- The two ports will be fed with the same amplitude to ensure proper mode generation. Therefore, they will be connected to a Wilkinson splitter. Since the lines face opposite directions, the phase difference will be 180 degrees, as needed.
- The radiating element. Here, it is the cylinder outer walls which the slots imprints directly the mode on.

However, the microstrip line presented in [19] is planar. An additional challenge arises from its conformation to the inner walls of the cylinder.

Finally, the slots are filled also with polyethylene to keep it as a sealed object. As a result a unique polyethylene piece incorporating the slot filling and the microstrip component is manufactured (Fig. 11). Two are necessary for each side of the cylinder. The piece is connected to the walls thanks to extensions allowing screw fixations. After that it is possible to match the antenna by modifying the length and width of the microstrip line [18]. A 50-Ohms line portion was added to allow fixation of a connector at its end. The 50-Ohms line portion is 5 mm long and 4 mm wide.

The advantage of this technique is the possibility of feeding multiple slots at the same time. Coupling is also reduced between slots (see Table. 3). Additionally, once the slots are etched, the metallic structure remains unchanged. All impedance matching is subsequently achieved through adjustments to the feeding line dimensions, enhancing the antenna's robustness and reproducibility. However, contrary to patches fed in serial, it is only possible to feed few slots using this technique. In fact, the end of the feeding line can be considered as a stub [20], however when adding more and more slots, it is difficult to match all the slots only with one end stub, the farthest slots eventually become completely mismatched. This could be overcome by adding other matching element on the line. Another point is the phase and amplitude feeding requirement. In case of design #1, the slots per microstrips need to be fed in phase. However, the phase on the feed line varies, and if the slots are too far apart (more than $\lambda_g/2$), the resulting phase shift will have too significant an impact on the excitation of the mode. Some slots could end up being fed out of phase, potentially generating a higher-order mode (the J_2 radial for example). It is possible to overcome that by using phase delays or meanders [21]. The amplitude dimension is also important, if the number of microstrip is too important, it is possible that there would be no more energy left at the end of the line to feed the last slot. It is possible to adjust by tuning the conductivities of the slots in order to limit the amount of energy absorbed by each one [21].

2.5.2.2. Design #3 (shunt feeding)

Unlike the design in the previous section, the slots will be fed in parallel. In this case by applying corporate feeding techniques [21]. For the sake of brevity, the design and optimization of the circuit are not addressed here. The final circuit requires only one port.

3. Results

3.1. Design #1

3.1.1. Simulation results

- **Bandwidth and far field results**

Each microstrip line is fed by a waveguide port (Fig. 11). The ports are connected via a Wilkinson splitter to achieve a single-port configuration. A bandwidth of 143 MHz (Fig. 17a) is obtained for the S_{11} of the combined ports (equivalent to the active S_{11}). It represents a fractional bandwidth (FBW)

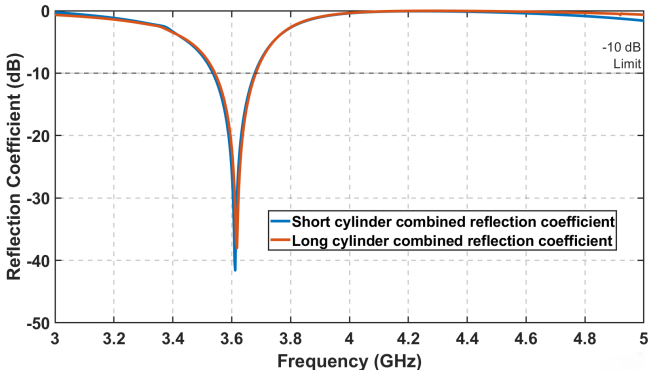

(a) S_{11} of Design #1 vs Design #1 with $12\lambda_c$ long carrier

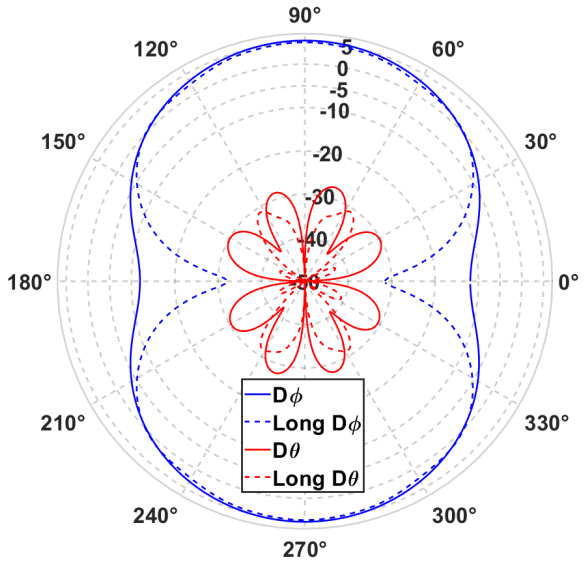

(b) Simulated x0z radiation pattern for Design #1 vs a $12\lambda_c$ long carrier @3.6 GHz

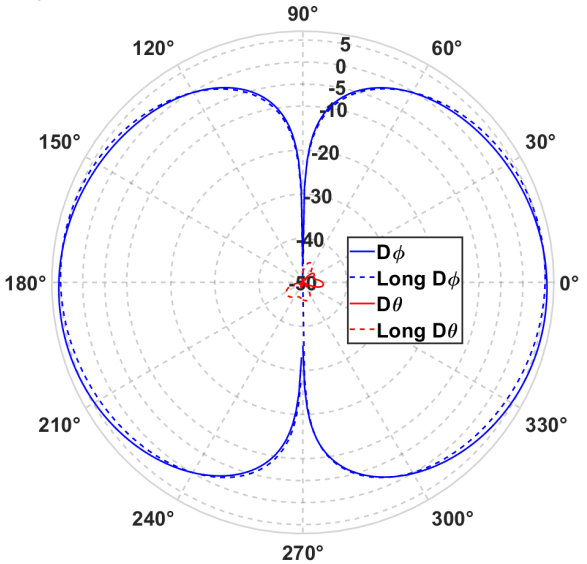

(c) Simulated x0y radiation pattern for Design #1 vs a $12\lambda_c$ long carrier @3.6 GHz

Figure 17: S parameter of normal Design #1 vs with $12\lambda_c$ length and associated 3D Far field

of 3.6%. Furthermore, a single lobe is produced on each side of the carrier. The correct diagram of the desired J_1 mode is obtained. A gain of approximately 5.5 dBi is obtained (Fig.17b and Fig.17c).

- **Interesting properties**

It can be noted that, the properties of quasi-insensibility used in [8] are conserved as shown on the same result graphs in Fig.17 for a length of $12\lambda_c$ (long carrier). It is possible to modify the length without significantly affecting the S-parameters or the x0y-plane radiation pattern. However, on the x0z cut (Fig. 17b), the radiation pattern is still impacted by the length change. Indeed, the long cylinder radiation pattern curve has a lower null level compared to the $1.2\lambda_c$ design. This will be further investigated in section 3.2.2.

3.1.2. Prototype results

A prototype was manufactured and characterized at the ISL. The microstrip was 3D printed and a copper line was affixed to it (Fig.18a). In terms of S_{11} (Fig.18b), the resonance frequency is shifted to 3.2 GHz with a bandwidth of 171 MHz (5.3%). A peak gain of 4 dBi at 3.2 GHz and similar radiation pattern are obtained (Fig.19). A reduction in the total efficiency of the measured antenna (Fig.18c) is observed.

It could be explained by flaws in the coaxial to microstrip solderings that can introduce impedance mismatches, signal losses, and perturbations in the total current distribution. There could also be air gaps between the 3D-printed microstrip lines and the inner walls of the cylinder. The 3D printed ε_r can also be slightly different. Taking these factors into account will undoubtedly improve the prototype performances.When simulating the impact of dielectric permittivity inaccuracies, it is observed that the resonance frequency increases inversely with the relative permittivity, at an approximate rate of 2.7% frequency shift per 10% variation in permittivity. Additionally, air gaps lead to an increase in the resonance frequency. Each millimeter of air gap introduced between the inner wall of the cylinder and the polyethylene substrate results in an approximate 0.5% increase in the resonance frequency. In terms of electric losses (loss tangent), no significant influence on the resonance frequency was found. Other unmodeled factors that may contribute to the observed shift include the soldering imperfections, particularly the thermal impact on the polyethylene substrate during the soldering process.

3.2. Design #2

3.2.1. Matching bandwidth and far field results

A bandwidth of 254 MHz (Fig. 20a) is obtained for the S_{11} after the Wilkinson splitter. It represents a fractional bandwidth of 6%. Furthermore, higher-order modes are consistently effectively eliminated, resulting in the achievement of a single lobe on each side of the carrier (Fig. 20b). A gain of approximately 5.76 dBi is obtained.

3.2.2. Interesting properties based on current isolation

The current is well directed but concentrated only at the vicinity of the slot (Fig. 15), at first glance, this seems like a significant disadvantage, as the directivity could be lower due to not fully

(a) Design #1 prototype parts

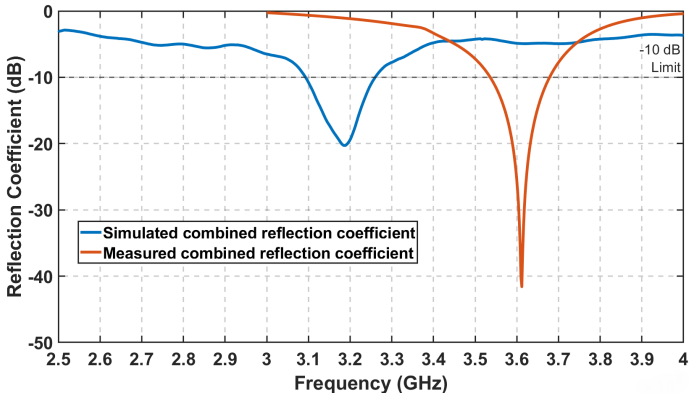

(b) Design #1 measure and simulation S_{11} vs frequency (GHz)

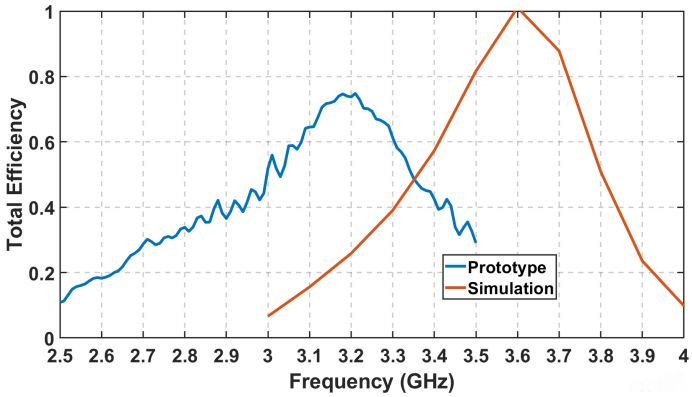

(c) Design #1 measure and simulation Efficiency vs frequency (GHz)

Figure 18: Design #1 prototype parts, efficiency and reflection coefficient results

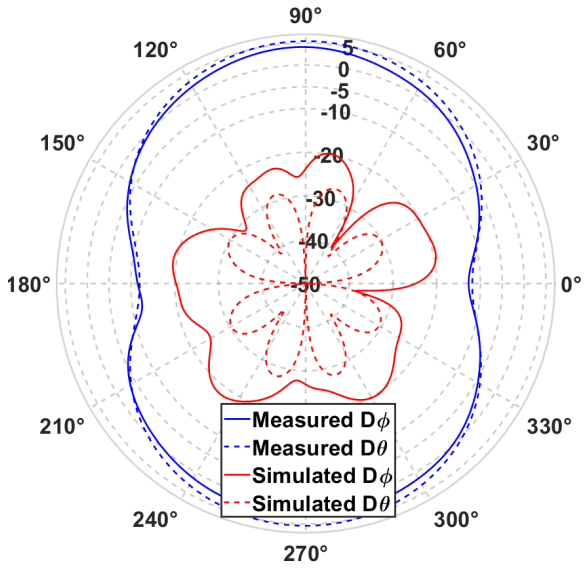

(a) Measured Radiation pattern @3.2 GHz vs Simulated @3.6 GHz at x0z

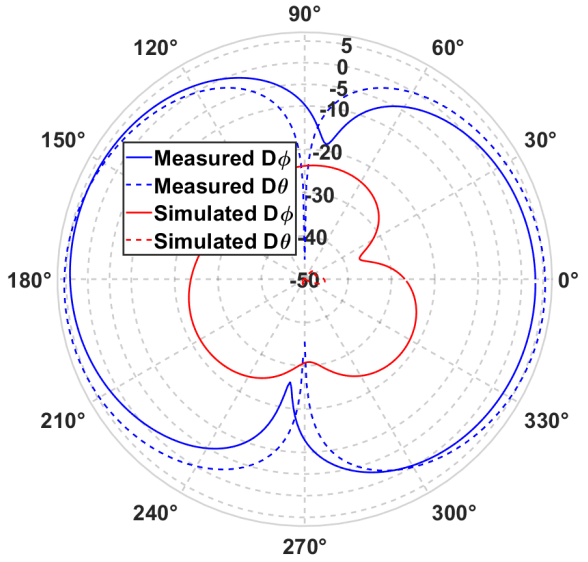

(b) Measured Radiation pattern @3.2 GHz vs Simulated @3.6 GHz at x0y

Figure 19: Design #1 radiation pattern measured @3.2 GHz vs Simulated @3.6 GHz radiation pattern results

utilizing the entire structure. However, it was determined that the quasi-insensitivity properties arise partly because the current is confined to only a subsection of the cylinder. This subsection, where the current is focused, is estimated to be 50 mm long. Two advantages emerge from this:

- This design can be applied to any type of carrier with the same radius, but with different lengths and/or antenna positions.
- As long as the subsection remains intact, the rest of the cylinder can be freely modified without affecting the radiation much. Except in the x0z plan when adding other radiating element like in [9], those elements will make more parts of the structures resonate and modify the radiation pattern in this plan.

This is shown by a parametric study of the far field when changing the length and even the position of the subsection along the cylinder (Fig. 21). On the x0y cut (radial cut), the same radiation pattern is obtained. However, On the x0z cut (length cut), as seen with design #1, the radiation pattern is still impacted by it. Indeed, the longer the length of the cylinder, the lower the null level (seen at 0 and 180° on Fig. 21a). This can be confirmed by examining the off-centered curve: on the

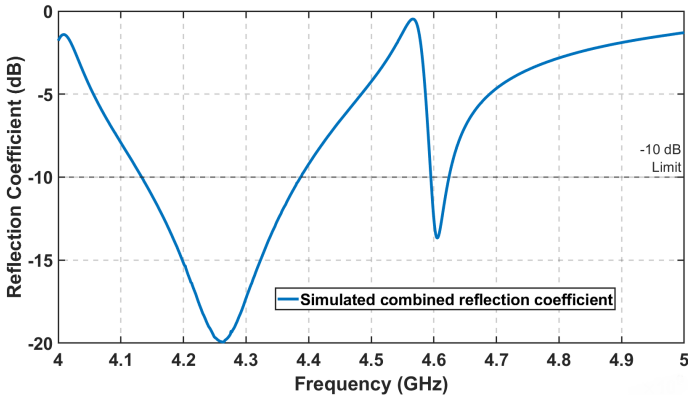

(a) Design #2 reflection coefficient in dB (S_{11}) versus frequency

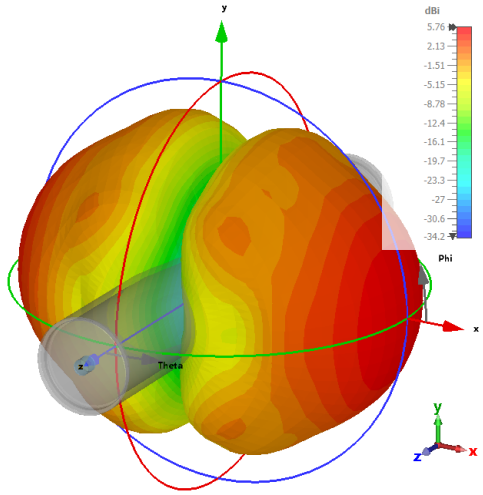

(b) Design #2 3D radiation pattern @4.3 GHz

Figure 20: Simulated reflection coefficient and radiation pattern results of design #2 @4.3 GHz

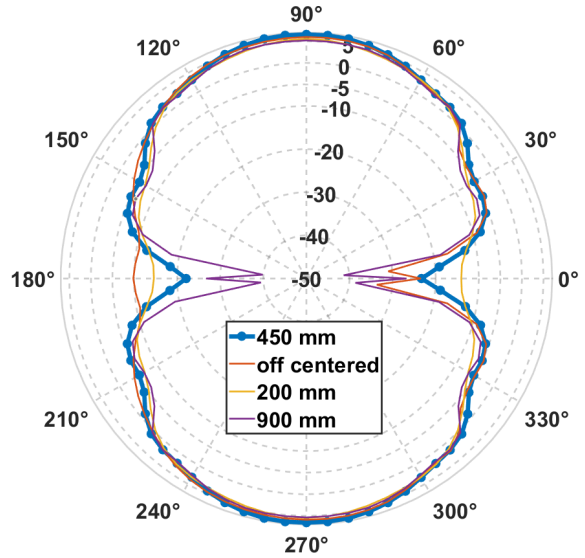

(a) Design #2 radiation pattern at YoZ when modifying the cylinder length @4.6 GHz

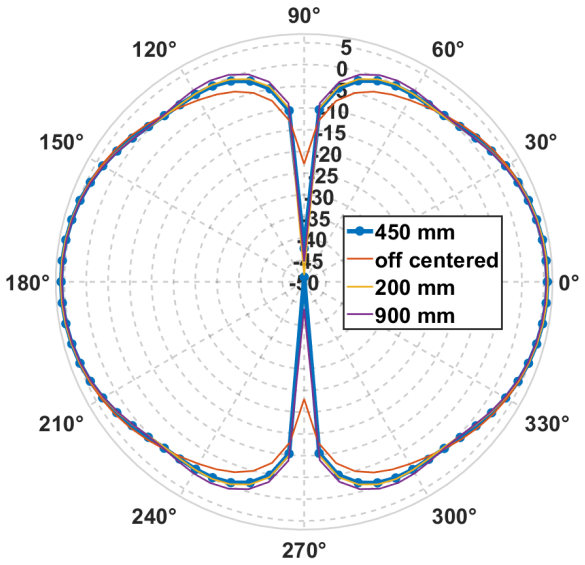

(b) Design #2 radiation pattern at x0y when modifying the cylinder length @4.6 GHz

Figure 21: Simulated directivity results when modifying the cylinder length or moving the subsection of design #2 @4.6 GHz

0° side, the null level is at -25 dB, while on the 180° side, it is only at -10 dB. However, the radiated mode is still the J_1 radial mode. Furthermore, parasitic slots may not exhibit the same level of efficiency when modifying the dimensions, as this time the matching was not always retained. Lastly, the authors have leveraged the property of quasi length insensitivity to design a structural antenna array, using these design #2 prototype subsections as unit antennas [9].

3.2.3. Prototype results

- **S parameter**

A prototype of design #2 has been manufactured and characterized (Fig. 22a). A frequency shift is observed and the measured bandwidth is centered at 4.6 GHz (Fig. 22b). A matching bandwidth of 350 MHz (7.6 %) is obtained.

- **Far field results**

In terms of far-field results (Fig.23), the prototype suffers from a 3.5 dBi loss of max gain at 4.6 GHz. The radiation pattern is preserved. However, as it was stated earlier, the feeding instabilities impacts the total efficiency of the prototype (Fig.24a) being only 60% at 4.6 GHz. The bad performances could also stem from inaccuracies in the simulation and manufacturing tolerances. Indeed, the numerical model employing discrete ports on slots placed along curvatures affects the convergence of the simulation. Furthermore, the asymmetries in the coaxial solderings are reflected in the asymmetries of the radiation graphs (Fig. 23b) .

- **Interesting property**

It is possible to see on the efficiency curve (Fig.24a) that there are some efficiency peaks reaching up to 80%, which is even higher than the main band. New wideband measurements have been conducted, revealing that these bands also appear in the wideband S-parameters (Fig.24b). Multiple bands exist

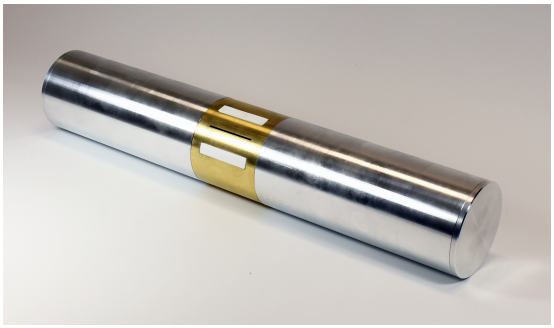

(a) Design #2 prototype fabricated at ISL

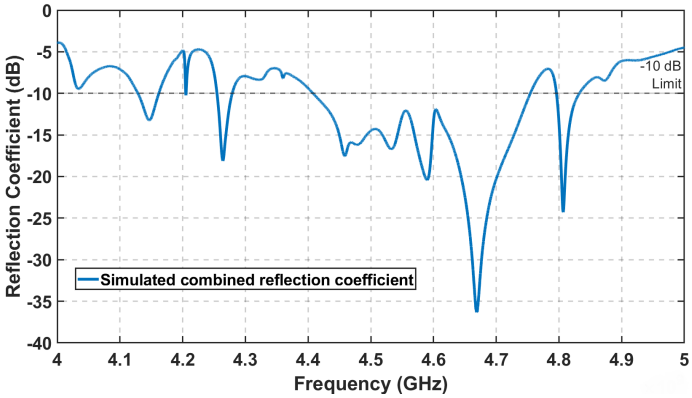

(b) Prototype combined reflection coefficient in dB vs. frequency

Figure 22: Design #2 prototype and associated reflection coefficient

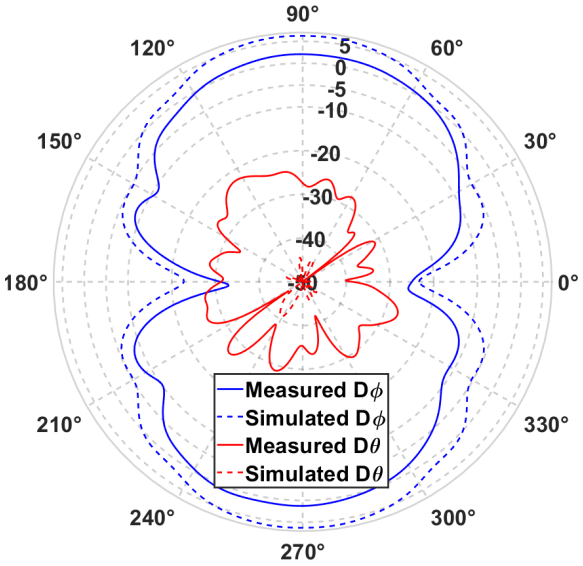

(a) Design #2 radiation pattern at YoZ @4.6 GHz vs simulated @4.3 GHz

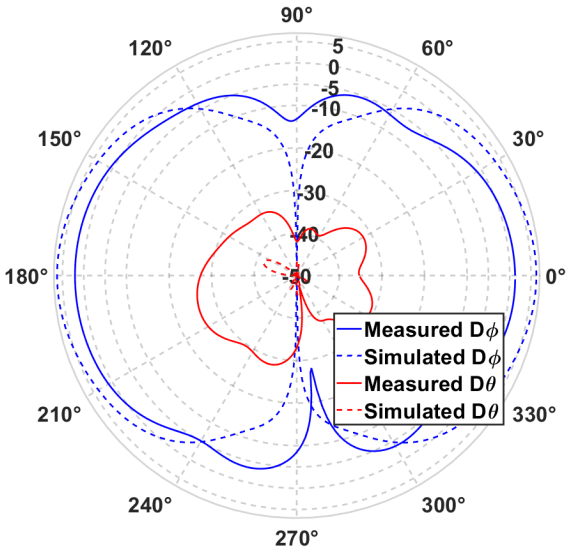

(b) Design #2 radiation pattern at x0y @4.6 GHz vs simulated @4.3 GHz

Figure 23: Design #2 measured realized gain results @4.6 GHz vs simulated @4.3 GHz

at 3.15 GHz (≈ 42 MHz), 3.55 GHz (≈ 30 MHz), 3.5 GHz (≈ 25 MHz), 4 GHz (≈ 20 MHz) but normally these would be corresponding to unusable higher order modes. However, when examining the diagrams, such as the 3.55 GHz radiation pattern (Fig.25), it is the same desired J_1 radial mode. That means that design #2 is multiband but monomodal. This is also the case for other bands (all bands are summarized in Table. 8). This property could be useful for frequency hopping applications or antenna mutualization. This multiband operation can be explained by the fact that at these different frequencies, we sufficiently suppress the higher-order modes, allowing the desired mode to resonate alone once again.

fc (GHz)	Band (MHz)	Max gain (dBi)	Desired mode ?
3.15	42	3.5	Yes
3.5	49	4	Yes
3.68	30	2.9	Yes
4	24	1.3	Yes
5.56	22	Not measured	?
5.7	183	Not measured	?
5.96	28	Not measured	?

Table 8: All design #2 new bands

3.3. Design #3

For Design #3, like design #2, multiple bands were obtained in simulation with matching bandwitdhs of 22 MHz at 2.3 GHz, 11 MHz at 2.48 GHz, 22 MHz at 2.66 GHz and 25 MHz at 2.88 GHz (Fig. 26a). However the desired mode was not preserved enough, with a sidelobe level of minimum 2 dB for the 2.48 GHz. Only the 2.3 GHz band is the J_0 radial mode (Fig. 27). In term of total efficiency, all four bands are also above 90%, so even if the radiation pattern is not perfectly omnidirectional, it can still be used for more directive communication.

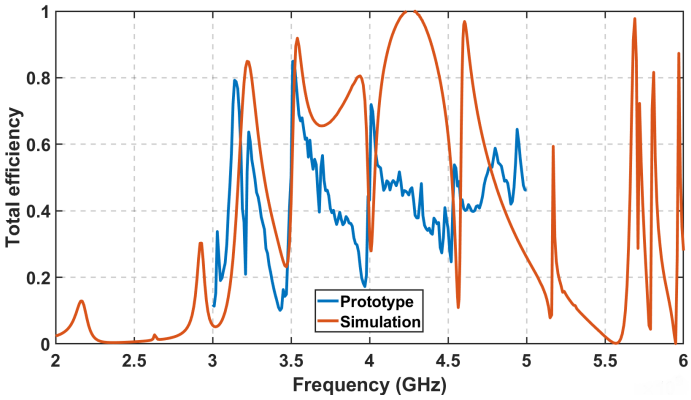

(a) Design #2 vs simulation total efficiency

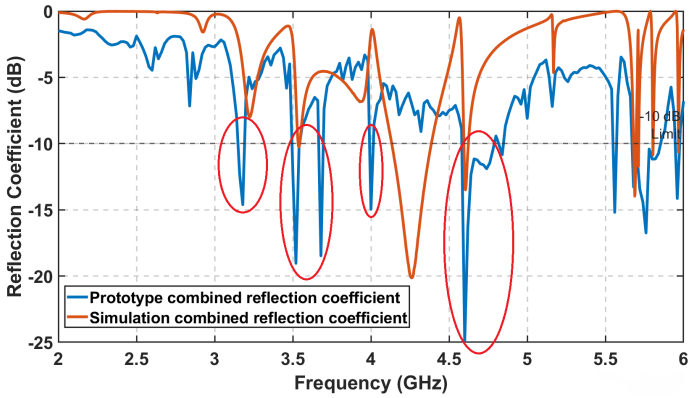

(b) Design #2 prototype wideband reflection coefficient vs simulation

Figure 24: Design #2 wideband prototype efficiency and reflection coefficient results

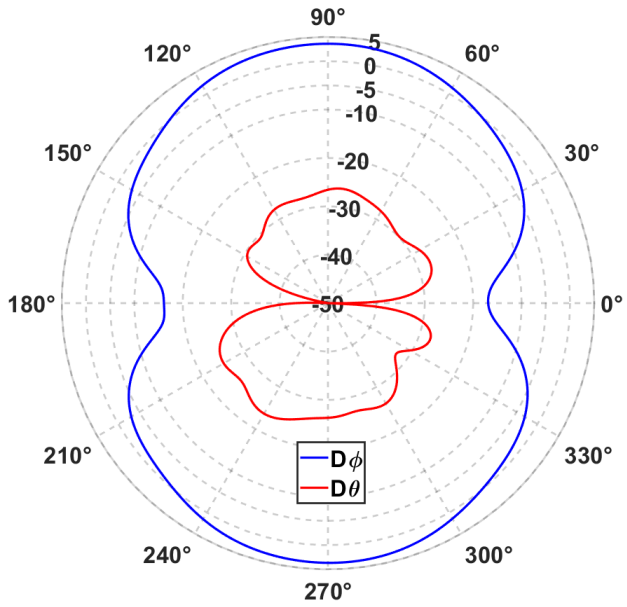

(a) Design #2 measured radiation pattern at YoZ @3.55 GHz

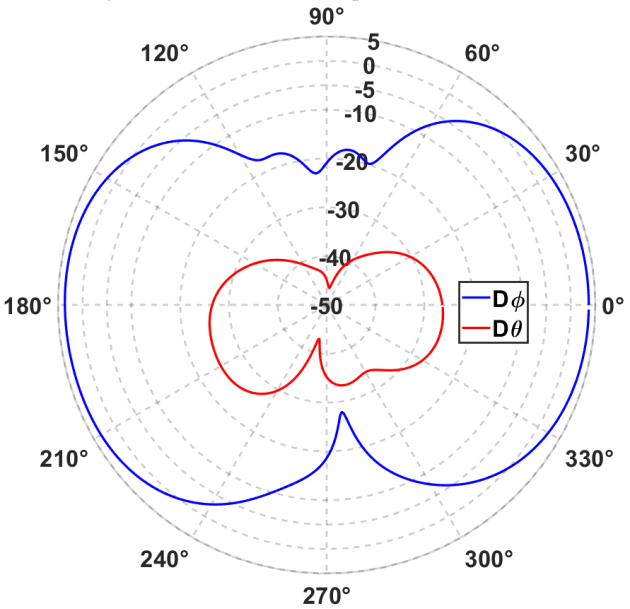

(b) Design #2 measured radiation pattern at x0y @3.55 GHz

Figure 25: Design #2 measured radiation patterns @2.3 GHz

4. Method summary

This section recaps the main results and contributions of the study, highlighting the effectiveness and applicability of the proposed design methodology. The methodology is as follows:

1. Modal investigation and mode selection
2. Mode excitation and higher order modes mitigation
3. Antenna feeding selection

For each step, two implementation techniques were explored, each with its own advantages and disadvantages that is presented, for mode selection :

- Using the J_0 radial omnidirectional mode produces a simpler current distribution, but is more susceptible to higher order modes.
- Using the J_1 radial loop mode produces a more robust and directionnal mode, but the feeding mechanism is more complex.

For mode excitation/higher order mode mitigation:

- Plain slots are easy to fabricate, but are the most basic couplers.
- H-shaped slots focus the current more effectively and provide an additional degree of freedom for modifying the matching. However, they are more complex to implement.
- Parasitic slots suppress higher order modes without adding ports, but they require drilling extra holes in the supporting structure.

For Antenna feeding selection:

- Coaxial feeding is the simplest feeding method, but it cannot excite multiple slots simultaneously, and the solderings may impact the S-parameters if asymmetrical, potentially causing also instability.

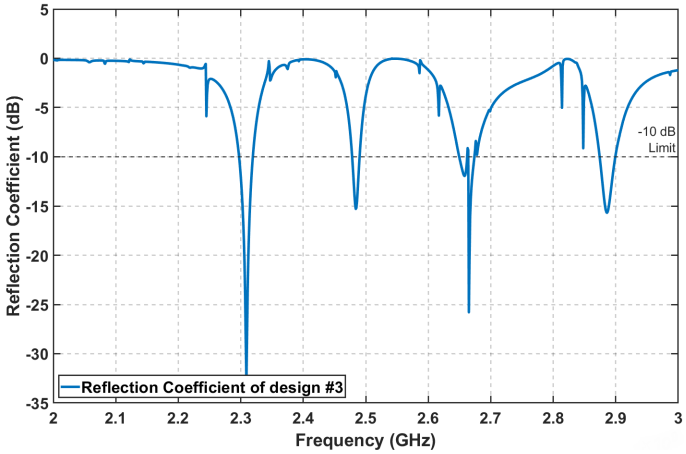

(a) Design #3 S_{11}

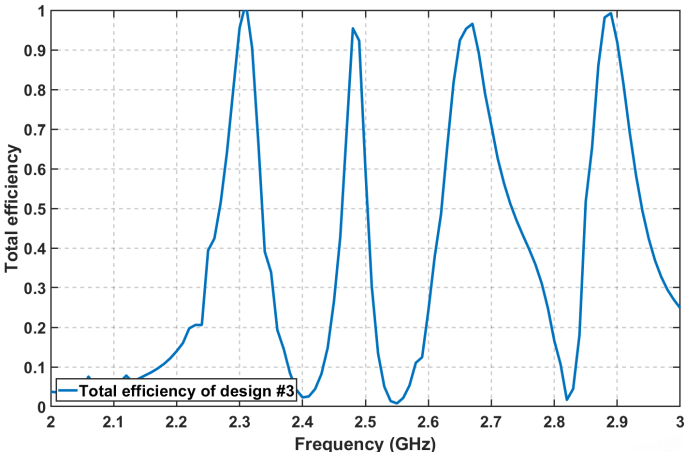

(b) Design #3 total efficiency

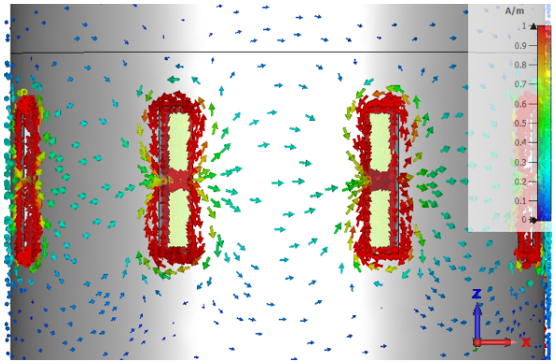

(c) Design #3 current distribution

Figure 26: Design #3 simulated reflection parameter, efficiency and current distribution

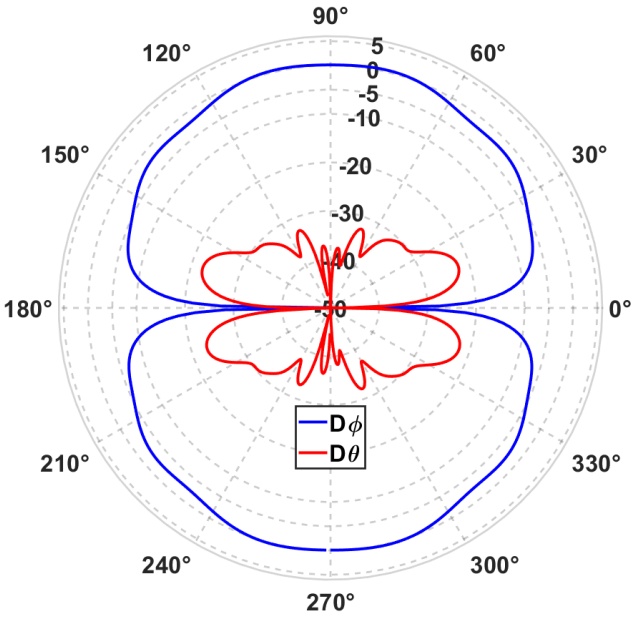

(a) Design #3 simulated radiation pattern at YoZ @2.3 GHz

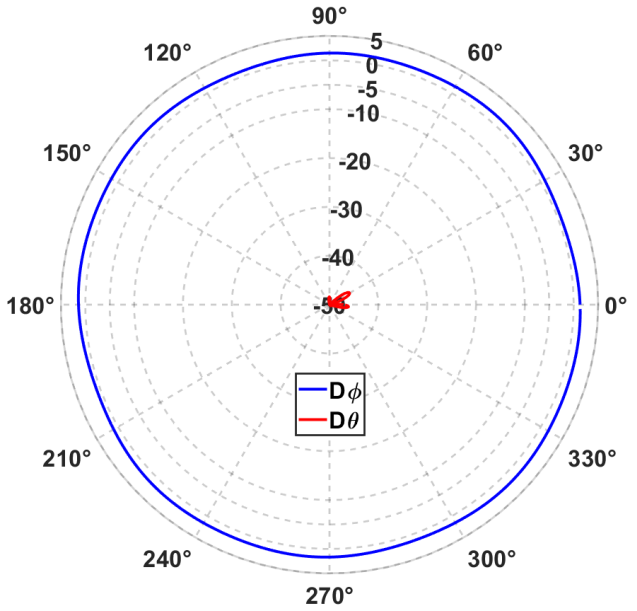

(b) Design #3 simulated radiation pattern at x0y @2.3 GHz

Figure 27: Design #3 simulated radiation patterns @2.3 GHz

- Microstrip aperture-coupled feeding is more complex but allows for the feeding of multiple slots simultaneously. Serial aperture-coupled feeding is the simplest method, though it is limited to exciting only a few slots at the same time. Parallel aperture-coupled feeding allows for more excitations but requires more space and is more complex to implement.

3 simulated designs and 2 prototypes were also shown:

- For Design #1 : 5.5 dBi and 3.6% bandwidth was obtained by simulation. The prototype gives us a peak gain of 4 dBi at 3.2 GHz and similar radiation pattern are obtained with also a 3.6% bandwidth. The correct mode is obtained, even if seven more resonant radial mode exist at the same frequency. However, a reduction in the efficiency is observed, the fabrication process must be improved in order to get better agreement between simulation and prototype.

- For Design #2 : A bandwidth of 254 MHz (6%) is achieved with a realized gain of approximately 5.76 dBi. The prototype provides a bandwidth of 350 MHz (7.6 %) with a max gain of 2 dBi. Asymmetries are also observed in the radiation pattern. The coaxial solderings must be

improved to achieve better agreement between the simulation and the prototype. The prototype is multiband and monomodal with 4 other bands summarized in Table. 8.

- For Design #3 : A simulated bandwidth of 22 MHz at 2.3 GHz with an omnidirectional pattern is obtained. The pattern is preserved only on this band even if three other simulated bands over 90% total efficiency. However, even if the patterns are degraded, it should be possible to still use them.

5. Conclusion and outlook

A cylindrical structural antenna systematic methodology for various radii and lengths comparable to or greater than the wavelength is proposed. Three distinct designs, differing in length, radius, excited modes, and feeding techniques, have been presented. Two of these were prototyped and experimentally evaluated to assess their properties. A comprehensive summary of the results is provided in part 4.

Regarding the outlook of this paper, it is planned to improve the prototypes and measure them with length extensions to verify the insensitivity property experimentally. Further studies will focus on cylinders with larger radii, the use of alternative modes, and mode reconfigurability to enhance the method. In particular, the parallel aperture-coupled feeding mechanism will be refined, as it is crucial for achieving balanced excitation and reducing asymmetries in slot excitation.

Acknowledgment

This work was supported by the direction générale de l'Armement (DGA AID) and the French German Research Institute of St Louis (ISL). I would like to thank particularly, the NSC group and most particularly Mr Frederic Walter who helped manufacture all the final prototypes.

References

[1] Y. Chen and C.-F. Wang, "Platform-Integrated Antenna System Design Using Characteristic Modes," in *Characteristic Modes: Theory and Applications in Antenna Engineering*. Wiley, 2015, pp. 221–265. [Online]. Available: https://ieeexplore.ieee.org/document/8045353

[2] H. Li, Y. Chen, and U. Jakobus, "Synthesis, Control, and Excitation of Characteristic Modes for Platform-Integrated Antenna Designs: A design philosophy," *IEEE Antennas and Propagation Magazine*, vol. 64, no. 2, pp. 41–48, 2022-04. [Online]. Available: https://ieeexplore.ieee.org/document/9712281/

[3] A. Pascawati, P. Hazdra, T. Lonsky, and M. R. K. Aziz, "Excitation of a conducting cylinder using the theory of characteristic modes," *Radioengineering*, vol. 27, no. 4, pp. 956–960, 2018.

[4] G. Marrocco and L. Mattioni, "Naval structural antenna systems for broadband hf communications," *IEEE Transactions on Antennas and Propagation*, vol. 54, no. 4, pp. 1065–1073, 2006.

[5] R. Ma and N. Behdad, "A spatially confined, platform-based hf direction finding array," *IEEE Transactions on Antennas and Propagation*, vol. 70, no. 2, pp. 1298–1308, 2021.

[6] Y. Chen and C.-F. Wang, "Hf band shipboard antenna design using characteristic modes," *IEEE Transactions on Antennas and Propagation*, vol. 63, no. 3, pp. 1004–1013, 2015-03. [Online]. Available: http://ieeexplore.ieee.org/document/7008478/

[7] D. Zhang, Y. Chen, and S. Yang, "Platform characteristic-mode-based omnidirectional antenna design using convex optimization," *IEEE Transactions on Antennas and Propagation*, vol. 72, no. 4, pp. 3801–3806, 2024.

[8] R. Notter, S. Collardey, A. Sharaiha, L. Bernard, P. Pouliguen, and P. Karmann, "Design of optimized cylindrical structural antenna with quasi length insensitivity using cma," in *2024 18th European Conference on Antennas and Propagation (EuCAP)*, 2024, pp. 1–5.

[9] R. Notter, A. Sharaiha, B. Loïc, C. Sylvain, P. Philippe, and K. Paul, "Réseau d'antennes structurelles cylindriques avec quasi insensibilité à la longueur," in *23e Journées Nationales Microondes*, Antibes, France, Jun. 2024. [Online]. Available: https://hal.science/hal-05004955

[10] "CST studio Suite, "CST Microwaves Studio"," Dassault Systèmes, 2024. [Online]. Available: CST.com

[11] R. Garbacz and R. Turpin, "A generalized expansion for radiated and scattered fields," *IEEE Transactions on Antennas and Propagation*, vol. 19, no. 3, pp. 348–358, 1971-05. [Online]. Available: http://ieeexplore.ieee.org/document/1139935/

[12] R. Harrington and J. Mautz, "Theory of characteristic modes for conducting bodies," *IEEE Transactions on Antennas and Propagation*, vol. 19, no. 5, pp. 622–628, 1971-09. [Online]. Available: https://ieeexplore.ieee.org/document/1139999/

[13] E. Antonino-Daviu, M. Cabedo-Fabrés, M. Ferrando-Bataller, and M. Gallo, "Design of a multimode mimo antenna using the theory of characteristic modes," *Radioengineering*, vol. 18, no. 4, pp. 425–430, 2009.

[14] W. Li, Y. Zhao, X. Ding, L. Wu, and Z. Nie, "A wideband pattern-reconfigurable loop antenna designed by using characteristic mode analysis," *IEEE Antennas and Wireless Propagation Letters*, vol. 21, no. 2, pp. 396–400, 2021.

[15] R. Martens, E. Safin, and D. Manteuffel, "Inductive and capacitive excitation of the characteristic modes of small terminals," in *2011 Loughborough Antennas & Propagation Conference*. IEEE, 2011-11, pp. 1–4. [Online]. Available: http://ieeexplore.ieee.org/document/6114141/

[16] R. Valkonen, A. Lehtovuori, and D. Manteuffel, "Capacitive coupling elements—changing the way of designing antennas," in *The 8th European Conference on Antennas and Propagation (EuCAP 2014)*. IEEE,

2014-04, pp. 229–233. [Online]. Available: http://ieeexplore.ieee.org/document/6901732/

[17] D. Manteuffel and R. Martens, "Compact Multimode Multielement Antenna for Indoor UWB Massive MIMO," *IEEE Transactions on Antennas and Propagation*, vol. 64, no. 7, pp. 2689–2697, 2016-07. [Online]. Available: http://ieeexplore.ieee.org/document/7431947/

[18] C. A. Balanis, *Antenna theory: analysis and design*. John wiley & sons, 2016.

[19] A. Kumar, J. Kaur, and R. Singh, "Performance analysis of different feeding techniques," *International journal of emerging technology and advanced engineering*, vol. 3, no. 3, pp. 884–890, 2013.

[20] R. Garg, *Microstrip Antenna Design Handbook*, ser. Antennas and Propagation Library. Artech House, 2001. [Online]. Available: https://books.google.fr/books?id=_er1LO5pEnUC

[21] R. Sainati, *CAD of Microstrip Antennas for Wireless Applications*, ser. Antennas and Propagation Library. Artech House, 1996. [Online]. Available: https://books.google.fr/books?id=86X35PUzY5IC